

Hierarchical EMC Analysis Approach for Power Electronics Applications

Dongsheng Zhao*, Braham Ferreira*, Anne Roch†, and Frank Leferink†‡

*Faculty of EWI, Delft University of Technology, Mekelweg 4, 2628CD, Delft, the Netherlands

Email: d.zhao@tudelft.nl Tel: +31 15 2785744

†Faculty of EWI, University of Twente, P. O. Box 217, 7500AE, Enschede, the Netherlands

‡Thales Netherlands, P. O. Box 42, 7550 GD, Hengelo, The Netherlands

Abstract - In this paper, a novel method for EMI (Electromagnetic Interference) level prediction is proposed. The method is based on the hierarchical structure of the generation of EMI. That is, the determination of EMI level can be divided into three levels, namely the functional level, the transient level and propagation level. The lower level provides parameter values for the higher level. That makes the analysis to be a single direction chain. In functional level, the working points are obtained. Through transient level analysis, the exact noise sources are determined. In propagation level, the high frequency characteristics in the propagation path are expressed including the variation of parasitic parameters. Frequency analysis can be used to get the EMI level measured in the receiver side rapidly. Because this approach is a straight forward method, the impact of any components can be evaluated immediately instead of doing the simulation from begin to end.

IndexTerms - EMI/EMC, Conducted emission, PWMVSI, motor drive, voltage source inverter

I. NOMENCLATURE

V_{dc}	voltage in dc-bus	[V]
V_{g+}	on-state gate voltage	[V]
V_{g-}	off-state gate voltage	[V]
V_{th}	gate threshold voltage	[V]
I_l	inductive load current	[A]
I_{rr}	diode peak reverse recovery current	[A]
R_g	IGBT gate resistor	[Ω]
g_m	IGBT transconductance	[S]
C_{ies}	IGBT input capacitance	[F]
C_{ge}	IGBT gate capacitance	[F]
L_s	IGBT stray inductance	[H]
t_{rr}	diode reverse recovery time	[s]

II. INTRODUCTION

A power electronics application is usually accompanied by high voltage and current amplitudes, steep voltage and current transients. The EMI (Electromagnetic Interference) issue is regarded as a main side effect for power electronics applications. Noise level prediction is a vital task for filter design, but many difficulties are encountered. For instance, the prediction asks many experiences to build equivalent circuit, using simplified model frequently loses high frequency details, individual approach must be developed for various topologies, etc. A universal method for EMI prediction of power electronics applications is desirable.

The universal method should overcome these common characteristics of power electronics application: (a) the large difference between the time constants [1], (b) the long time before reaching steady state. Doing simulation in time domain is very time-consuming. Using frequency domain approach needs to assume the periodic noise source and fixed propagation path, which is not true. For instance, the slopes of voltage and current transient depends on the operation conditions, the assumption of periodic noise source does not exist. Because the junction capacitors of grid rectifiers change with the reverse voltage [2], the noise propagation path is not fixed as well. A hierarchical approach combines the advantage of the time domain and frequency domain approach to achieve a fast, universal and accurate prediction is desirable.

In this paper, the approach is described with detail, then a PWM voltage source inverter feeds an induction motor is analyzed by this approach because it is a typical power electronic application. The result is given and compared with experiment result. The comparison verifies the feasible and advantages of the approach. The comparison is also done to compare this approach to conventional methods, in the aspect like speed and accuracy.

III. HIERARCHICAL STRUCTURE

The determination of EMI level can be divided into three levels, namely the functional level, the transient level and propagation level. The lower level provides parameter values for the higher level. In functional level, the working points are obtained. Through transient level analysis, exact noise sources are determined. In propagation level, the high frequency characteristics in the propagation path are expressed including the variation of parasitic parameters.

A. Functional Level

In functional level, the switches are idealized, which have the following characteristics:

- transient time is zero for turning on and turning off;
- the conducted impedance is zero when the switch turns on, and is infinite large when the switch turns off.

The circuit is further simplified by ignoring parasitic parameters in the circuit. These simplifications make the mathematical modelling and analysis feasible. The operation conditions can also be determined by analytic approach. In frequency

domain, the calculation in this level gives the correct frequency spectrum in the low frequency range part. In high frequency range part, the levels are overestimated because the transients are idealized by zero transient time. Therefore, a correction factor is needed.

B. Transient Level

As we know, the real signal around the transition can be described very close to the real behaviour by the convolution of two waves in the time domain. The first one is the piecewise linear waveform obtained in the functional level. The second one is the derivative of the signal in transition.

The signal in transient is the current and voltage transient of the switches. Their waveforms are determined by the operation condition of the switches. That means the waveforms change at each transient. In Figure 1, a measurement is done for the voltage waveform during a commutation, the trigger is set to different current level and in a small range. It can be observed easily, that the dv/dt changes significantly with the load current.

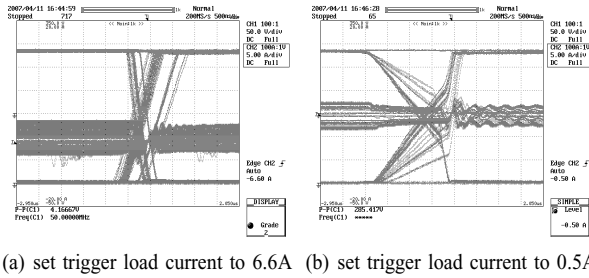


Fig. 1. The voltage transient slope changes with load current

C. Propagation Level

Known from [2], the effect of the equivalent capacitance when the grid rectifiers turn-off is notable in conducted frequency band. Also, all the switching devices and load have their inner passive parasitic components, they are included as a part of propagation path. The transfer ratio is defined as the ratio between the voltage drop over the LISN 50Ω resistor and the noise source.

D. Flow Chart of Hierarchical EMC Analysis Approach

The procedures of hierarchical EMC analysis approach are summarized in Figure 2 shown below. In the flowing sections, hierarchical EMC analysis approach is applied to predict the EMI level of a variable speed motor drive system. The explanations are available in next sections.

IV. IMPLEMENT STEPS IN FUNCTIONAL LEVEL

The inverter circuit is operated by a sinusoidally pulse width modulated signal to produce an output. The purpose in this level is to get the right voltage and current waveforms by analytical approach. The steps are listed below.

- 1) The fundamental and harmonics of output voltage are calculated.

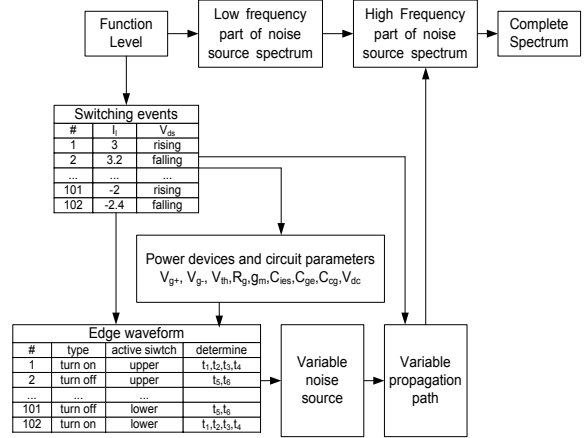


Fig. 2. Flow chart of hierarchical EMC design procedures

- 2) The parameters of low frequency induction motor model are achieved via experiment measurement.
- 3) The fundamental and harmonics of output current are derived via the equivalent circuit.
- 4) The waveform of input current is reconstructed.
- 5) The operation condition of the current and voltage in each switching event are recorded.

A. PWM Output Voltage Spectrum

The procedure to calculate the harmonic components of PWM output voltage in an analytical way can be found in many literature, like [3], [4]. The benefit is that the relationship between the amplitude of harmonic components and variables can be expressed by close-form equations. This approach use double fourier integral approach to express the PWM switched waveform by an infinite series of two-dimensional sinusoidal harmonics.

$$f(t) = A_{00} + \sum_{n=1}^{\infty} [A_{0n} \cos(n\omega_0 t) + B_{0n} \sin(n\omega_0 t)] + \sum_{m=1}^{\infty} \sum_{n=-\infty}^{\infty} [A_{mn} \cos((m\omega_c + n\omega_0)t) + B_{mn} \sin((m\omega_c + n\omega_0)t)]$$

The coefficients can be calculated by,

$$A_{mn} = \frac{1}{2\pi^2} \int_{-\pi}^{\pi} \int_{-\pi}^{\pi} f(x, y) \cos(mx + ny) dx dy$$

$$B_{mn} = \frac{1}{2\pi^2} \int_{-\pi}^{\pi} \int_{-\pi}^{\pi} f(x, y) \sin(mx + ny) dx dy$$

Where, $x = \omega_c t$, $y = \omega_0 t$.

An alternative approach is using FFT method, which is approved to be faster and more efficient. The waveform can be calculated according to the PWM schemes. Then, the waveform is converted to frequency domain via FFT method. The FFT module is very common and the algorithm has already

been optimized to support large scale and quick calculation. Therefore, the output voltage is expressed by,

$$f(t) = \sum_{n=-\infty}^{\infty} C_n e^{\frac{2\pi j n}{T} t} \quad (1)$$

Via these two approaches, the frequency spectrum can be obtained.

B. The parameters of low frequency induction motor model

For fundamental and harmonic frequency of output voltage, the equivalent circuit is shown in Figure 3.

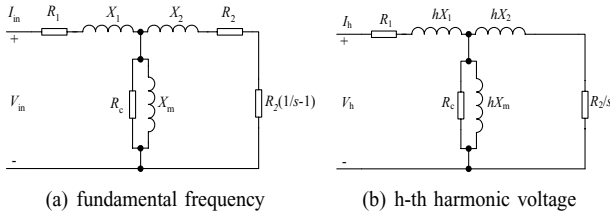


Fig. 3. Per-phase equivalent circuit

Exact values of the parameters in the model of induction motor can be extracted using experimental method. A standard test procedure for this measurement is suggested by [5]. The fractional slip s changes with the mechanical load.

The torque-slip relationship can be expressed by [6]:

$$T_{mech} = \frac{1}{\omega_s} \left[\frac{n_{ph} V_{1,eq}^2 (R_2/s)}{(R_{1,eq} + (R_2/s))^2 + (X_{1,eq} + X_2)^2} \right] \quad (2)$$

Here,

$$V_{1,eq} = V_{in} \left(\frac{jX_m}{R_1 + j(X_1 + X_m)} \right) \quad (3)$$

$R_{1,eq}$ and $X_{1,eq}$ are the real and imaginary part of $Z_{1,eq}$.

$$Z_{1,eq} = \frac{jX_m(R_1 + jX_1)}{R_1 + j(X_1 + X_m)} \quad (4)$$

The curve is drawn with load characteristic. The cross point is the working point when steady-state is reached. With the known ω_m , the s is known for certain load and the model for the fundamental and harmonic frequency is complete.

C. PWM Load Current Waveform

The fundamental and harmonic component of PWM output current can be derived from the complete model above. Here the motor leakage reactances X_1 and X_2 are assumed to be invariant with the frequency.

With the frequency spectrum and phase information of the output current, the waveform of the output current can be reconstructed via inverse FFT.

D. Switching Events

We get the current and voltage waveforms from the analysis in previous level. In the voltage source inverter, the switching events occur at each voltage transient. The informations of operation points are recorded with each switching event.

Here gives partial examples inside a switching events file. The load current is obtained from the current waveform. The source voltage at the moment when transient occurs are also recorded. That is used to calculate the reverse biased voltage of the rectifier diodes which have influence to the noise propagation path.

TABLE I
EVENTS LIST EXAMPLE

Event	I_l	Vsa	Vsb	Vsc
10	-22.0	24.8	-281.0	256.2
11	8.1	29.7	-283.1	253.4
12	22.8	33.0	-284.4	251.4
13	18.5	35.1	-285.3	250.2
14	-4.0	38.2	-286.5	248.2
15	-24.7	43.3	-288.5	245.2

When the commutation happens between a transistor and a diode. The transistor is called active switch. The identification follows these rules:

$$\text{Active switch is } \begin{cases} \text{upper switch} & \text{when } I_l > 0 \\ \text{lower switch} & \text{when } I_l < 0 \end{cases}$$

The switching events are classified into two types, that is turn-on and turn-off. It is necessary to identify them because the slopes of these transients are calculated respectively. The identification criteria are list below:

$$\text{sw. event } \begin{cases} \text{upper sw. turns on} & \text{when } I_l > 0 \text{ and } V_{ds} \text{ rises} \\ \text{upper sw. turns off} & \text{when } I_l > 0 \text{ and } V_{ds} \text{ falls} \\ \text{lower sw. turns off} & \text{when } I_l < 0 \text{ and } V_{ds} \text{ rises} \\ \text{lower sw. turns on} & \text{when } I_l < 0 \text{ and } V_{ds} \text{ falls} \end{cases}$$

The types of transients are identified.

TABLE II
EVENTS LIST EXAMPLE (CONT.)

Event	Type	V in active leg	V in other two legs
10	turn-on	-253.8	253.8 253.8
11	turn-off	-253.8	-253.8 253.8
12	turn-off	-253.8	-253.8 -253.8
13	turn-on	253.8	-253.8 -253.8
14	turn-off	253.8	-253.8 253.8
15	turn-off	253.8	253.8 253.8

V. TRANSIENT LEVEL

The switching transient in a power converter has traditionally been analyzed by modelling it as a fixed slope dv/dt and di/dt transient. Actually, this switching transient is a superposition of multiple slopes [7], further more, these slopes changes with the load current. The operation condition of the switches determines the transient edge.

To avoids the excessive approximation that noise signal is periodic, for the high frequency noise source, the operation points should be taken into account.

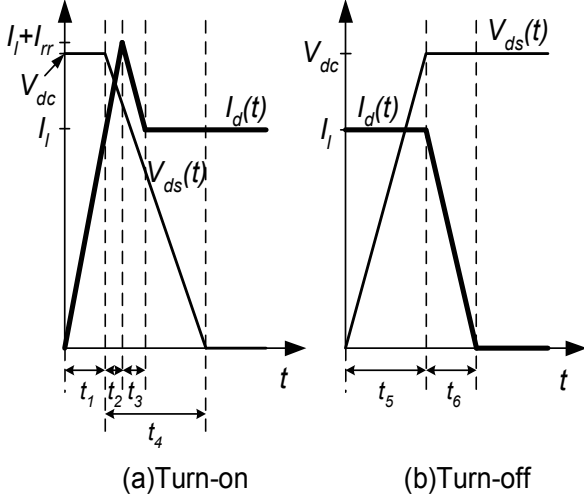


Fig. 4. Switching waveform

A. Determine the Transient Waveforms

For each IGBT transient events, the waveforms are sketched in Figure 4. The nonlinear switching transient model is based on the discussion in [7]. The slow transients are ignored because it has been proved by simulation that ignoring these slow transients would not have significant influence to the noise frequency spectrum. The turn-on transient which is illustrated in the left figure is first analyzed.

During t_1 , the I_d increases in a slope which can be calculated by Equation 5.

$$\left(\frac{dI_d}{dt}\right)_{t_1} = \frac{g_m V_{g-} - V_{th} - I_l/g_m}{R_g C_{ies} + g_m L_s} \quad (5)$$

The g_m can be derived from the typical transfer characteristic curve in datasheet by

$$g_m = \frac{\Delta I_d}{\Delta V_{ge}} \quad (6)$$

The duration of t_1 is calculated by,

$$t_1 = I_l / \left(\frac{dI_d}{dt}\right)_{t_1} \quad (7)$$

In most datasheets of IGBT, the diode reverse recovery time t_{rr0} and peak reverse current I_{rr0} are measured under a standard test configuration with I_F and $\frac{dI_F}{dt}$. From [8], the following relationships exist,

$$t_{rr}, I_{rr} \propto \sqrt{I_d} \quad (8)$$

$$1/t_{rr}, I_{rr} \propto \sqrt{\left(\frac{dI_d}{dt}\right)_{t_1}} \quad (9)$$

We can calculate t_{rr} and I_{rr} by,

$$I_{rr} = I_{rr0} \sqrt{\frac{I_l \left(\frac{dI_d}{dt}\right)_{t_1}}{I_F \left(\frac{dI_F}{dt}\right)}} \quad (10)$$

$$t_{rr} = t_{rr0} \sqrt{\frac{I_l \left(\frac{dI_F}{dt}\right)}{I_F \left(\frac{dI_d}{dt}\right)_{t_1}}} \quad (11)$$

During t_2 , the I_d changes from I_l to $I_l + I_{rr}$ with the same slope.

$$\left(\frac{dI_d}{dt}\right)_{t_2} = \left(\frac{dI_d}{dt}\right)_{t_1} \quad (12)$$

The time duration for I_d rushing to the top is

$$t_2 = I_{rr} / \left(\frac{dI_d}{dt}\right)_{t_2} \quad (13)$$

The time for I_d backing to the I_l is

$$t_3 = t_{rr} - t_2 \quad (14)$$

During t_4 , the V_{ds} decreases to zero in a slope of

$$\left(\frac{dV_{ds}}{dt}\right)_{t_4} = \frac{-1}{C_{cg}} \left\{ \frac{V_{g+} - V_{th} - I_l/g_m}{R_g} + \frac{C_{ge}}{g_m} \left(\frac{dI_d}{dt}\right)_{t_1} \right\} \quad (15)$$

The duration of t_4 is calculated by,

$$t_4 = V_{dc} / \left(\frac{dV_{ds}}{dt}\right)_{t_4} \quad (16)$$

The turn-off transient which is illustrated in the right figure can be analyzed below. During t_5 , the V_{ds} increases from zero to V_{dc} , the slope is,

$$\left(\frac{dV_{ds}}{dt}\right)_{t_5} = \frac{g_m V_{g-} - V_{th} + I_l/g_m}{R_g C_{cg}} \quad (17)$$

The duration of t_5 is calculated by,

$$t_5 = V_{dc} / \left(\frac{dV_{ds}}{dt}\right)_{t_5} \quad (18)$$

The overvoltage of V_{ds} is ignored in the noise model. If the V_{ds} reaches V_{dc} , then the switch current I_d decays to zero.

$$\left(\frac{dI_d}{dt}\right)_{t_6} = \frac{g_m V_{g-} - V_{th} - I_l/g_m}{R_g C_{ies} + g_m L_s} \quad (19)$$

The duration of t_6 is calculated by,

$$t_6 = I_l / \left(\frac{dI_d}{dt}\right)_{t_6} \quad (20)$$

Also, the ‘‘tailing’’ of the drain current of IGBT is ignored here due to its low transient slope.

B. Transient Noise Source in Frequency Domain

The derivatives of the noise sources are first calculated. They are then transformed into s domain. The value is the correction factor to correct the overestimated high frequency part spectrum of the noise source.

The calculation is done after the types of transients are identified.

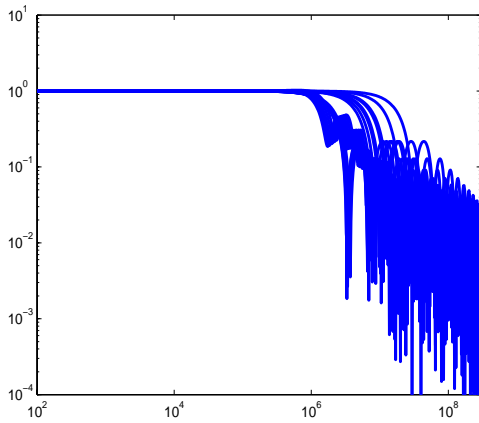
$$I_{on}(s) = \frac{1 + I_{rr}/I_l}{t_1 + t_2} \frac{1 - e^{-(t_1+t_2)s}}{s} - \frac{I_{rr}/I_l}{t_3} \frac{1 - e^{-(t_3)s}}{s} e^{-((t_1+t_2)s)}$$

$$V_{on}(s) = -\frac{1}{t_4} \frac{1 - e^{-(t_4)s}}{s} e^{-(t_1)s}$$

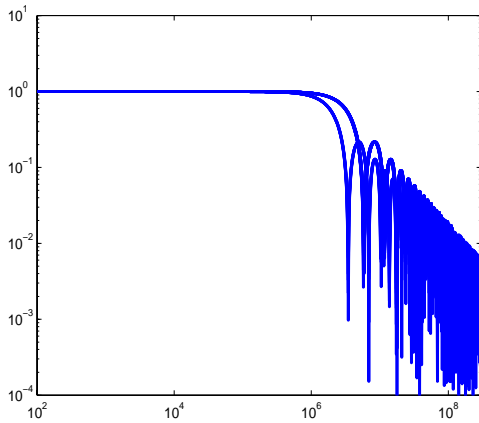
$$I_{off}(s) = -\frac{1}{t_6} \frac{1 - e^{-(t_6)s}}{s} e^{-(t_5)s}$$

$$V_{off}(s) = \frac{1}{t_5} \frac{1 - e^{-(t_5)s}}{s}$$

In Figure 5, the correction factors in many switching events are calculated and drawn. We do find the influence in different switching events.



(a) current



(b) voltage

Fig. 5. Noise source model, consider the variation of parasitic

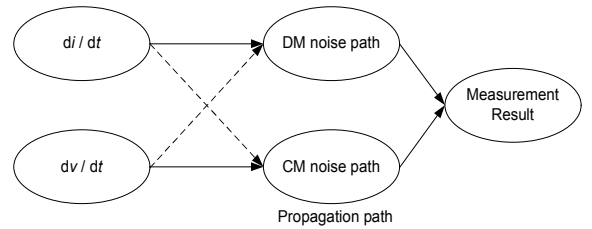
VI. PROPAGATION LEVEL

In this level, the noise cell can be created based on the waveforms obtained in previous level. Unlike simplified models in

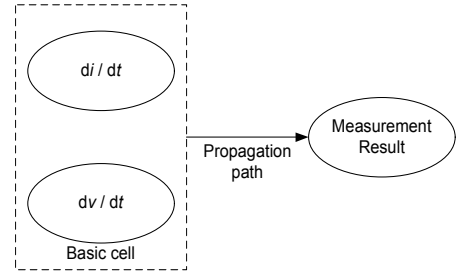
other's work, where the circuits are simplified into CM and DM equivalent circuit, the calculation is done on a complete circuit with fixed topology. transfer ratio is defined as the ratio between the voltage drop over the LISN 50Ω resistor and the voltage source and current source. This transfer ratio is calculated based on the operation condition information at each switching event to get more exact EMI level. The value of these parasitic elements is variable with operation points.

A. Basic Noise Cell

The equivalent circuits and noise models have been discussed for many times. Conventional approaches use voltage source to derive the CM noise and current source to derive the DM noise. This is a reasonable approximation for simplicity. In recent research works, some exemptions are found that the voltage source can generate DM noise, which is named MM noise [9], [10]. Also, the current source can generate CM current flowing through ground [11]. They are illustrated by dashed lines in Figure 6(a). A basic noise cell is proposed to get compromise between simplicity for calculation and completeness of model. We use complete circuits instead of simplified CM and DM equivalent circuits, shown in Figure 6(b).



(a) Conventional model



(b) The new proposed model

Fig. 6. Noise source model,

The approach is described here,

- The switching active components are the noise sources. The high di/dt and dv/dt associated with the switching actions is the main reason generating emission. They are modeled as voltage source and current source corresponding to fast transient of voltage and current.
- The flywheel diodes connected to the active components are controlled sources. The basic noise cell is shown in Figure 7.
- All parasitic components are included to get exact prediction. The diagram is shown in Figure 8.

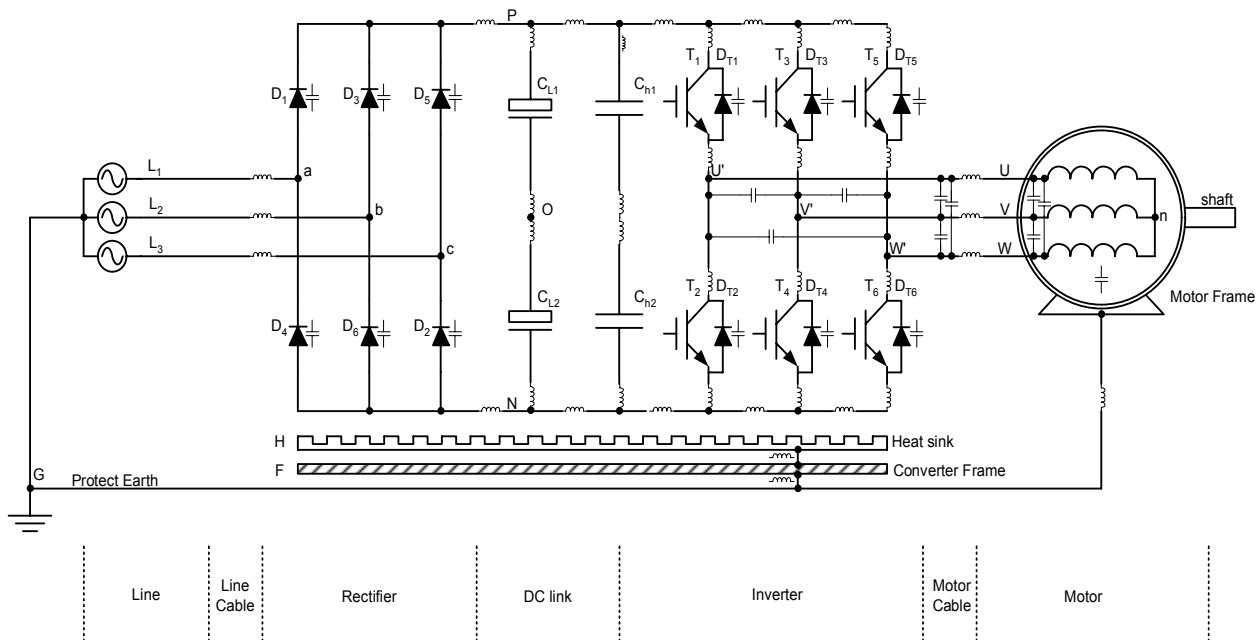


Fig. 8. Propagation path includes all parasitics

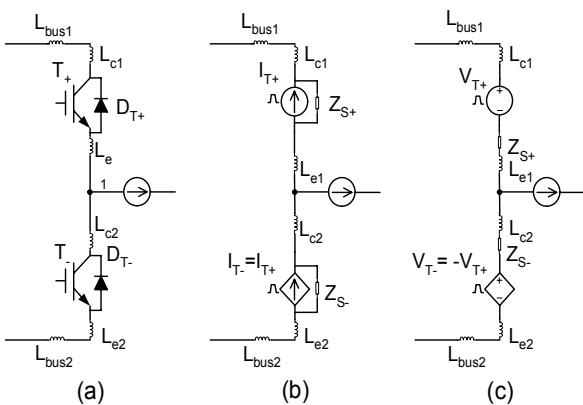


Fig. 7. Noise cell model; (a) diagram of inverter leg, (b) current noise source model, (c) voltage noise source model

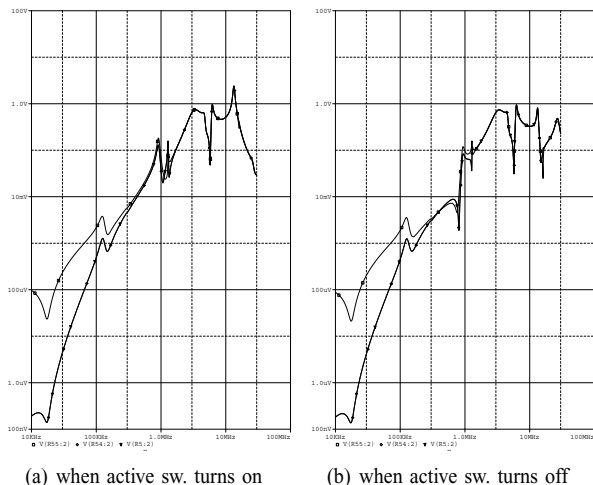


Fig. 9. Voltage source transfer ratio

Based on the circuit above, the transfer ratio is calculated for current noise source and voltage noise source respectively. Two switching events are selected when the active switch is upper switch, and the switch turns on and turns off.

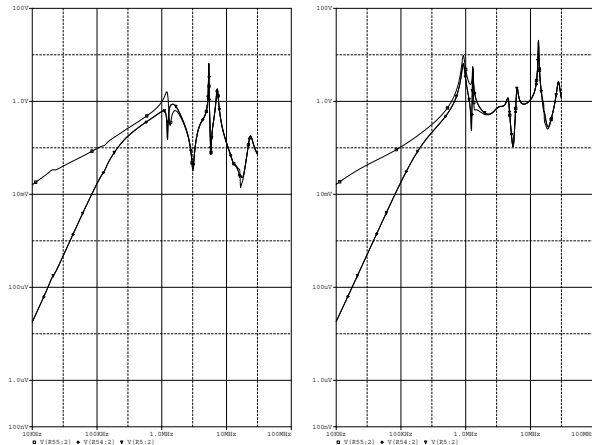
In each transfer ratio plot, the voltage source or current source is set to 1V or 1A. The voltage drops in the three 50Ω resistors in LISN are calculated. It is observed, that the conduct pattern of rectifier diodes does not have significant impact above 500kHz. While the states in inverter do change the transfer ratio even in high frequency range.

VII. VALIDATION

The experimental bench has been built to verify this method. It is designed to represent a typical variable speed drive system. The main elements are depicted here:

- line impedance stabilized network (LISN): 50Ω/50μH V-LISN used for compliant test of band B (150 kHz-30 MHz) defined in CISPR 16. LISN100A3P, 100A 3-Phase, Cranage EMC Tech. Ltd.;
- variable speed drive: Danfoss VLT5016. It is constituted by four IGBT modules (FUJI 2MBI 75S-120 2-Pack IGBT). Three of them are used for inverter legs. The remaining one is for motor braking;
- power bridge rectifier: SKD62/16, SEMIKRON;
- induction motor: Heemaf Holland BV, 3×380V/7.5kW, nominal speed: 1445/min 50Hz;

The noise source spectrum, correction factors and transfer ratio are combined together to predict the EMI level. It is compared to experiment result. The preliminary result is



(a) when active sw. turns on (b) when active sw. turns off

Fig. 10. Current source transfer ratio

shown below.

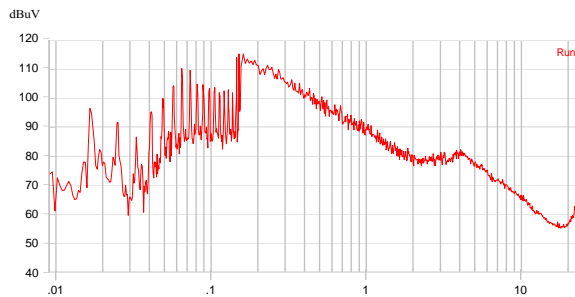


Fig. 11. LISN measurement result

VIII. CONCLUSIONS AND FURTHER RESEARCH

This paper presents a short introduction to the necessity of predicting conducted noise emission of power electronic converter and its difficulty. It proposes an approach to rapidly obtain the prediction of the EMI level with enough accuracy. It is realized via hierachical way. In functional level, large time

constant is used to get the working points of each switching devices. Then the switching devices are replaced by current noise source and voltage noise source. In transient level, the transient edges of the noise source are replaced by piece-wise linear lines using nonlinear switching transient model. The operation condition information achieved in the previous level is used to calculate the transient slope. In the propagation level, thanks to the established working points information, the characterization of propagation path is improved.

This approach is used in a voltage source inverter feeding a induction motor to predict the EMI level. Our research task is now oriented towards apply this approach to predict EMI level of a ZCS-CV inverter with variable switching frequency.

REFERENCES

- [1] P. Mugur, J. Roudet, and J. Crebier, "Power electronic converter EMC analysis through state variable approach techniques," *IEEE Trans. Electromagnetic Compatibility*, vol. 43, no. 2, pp. 229–238, 2001.
- [2] J. He, J. Jiang, J. Huang, and W. Chen, "Model of EMI coupling paths for an off-line power converter," *Applied Power Electronics Conference and Exposition, 2004. APEC'04. Nineteenth Annual IEEE*, vol. 2, 2004.
- [3] D. Holmes and T. Lipo, *Pulse Width Modulation for Power Converters: Principles and Practice*. IEEE Press, 2003.
- [4] D. Gonzalez, J. Gago, and J. Balcells, "New simplified method for the simulation of conducted EMI generated by switched power converters," *IEEE Trans. Industrial Electronics*, vol. 50, no. 6, pp. 1078–1084, 2003.
- [5] IEEE-SA Standards Board, "IEEE Standard Test Procedure for Polyphase Induction Motors and Generators," *IEEE Std 112-2004 (Revision of IEEE Std 112-1996)*, pp. 1–79, 2004.
- [6] A. Fitzgerald, S. Umans, and C. Kingsley Jr, *Electric Machinery*. McGraw-Hill Publishing Co., 2002.
- [7] J. Meng and W. Ma, "Power converter EMI analysis including IGBT nonlinear switching transient model," *IEEE Trans. Industrial Electronics*, vol. 53, no. 5, pp. 1577–1583, 2006.
- [8] N. Mohan, T. Undeland, and W. Robbins, *Power Electronics: Converters, Applications and Design*. John Wiley & Sons, Inc, 2003.
- [9] D. Zhang, D. Chen, and D. Sable, "Non-intrinsic differential mode noise caused by ground current in an off-line power supply," in *Proc. IEEE Power Electronics Specialists Conf. (PESC)*, vol. 2, pp. 1131–1133, 1998.
- [10] J. Meng and W. Ma, "A new technique for modeling and analysis of mixed-mode conducted EMI noise," in *Proc. IEEE Power Electronics Specialists Conf. (PESC)*, vol. 2, pp. 1679–1687, 2004.
- [11] X. Huang, "Frequency Domain Conductive Electromagnetic Interference Modeling and Prediction with Parasitics Extraction for Inverters," Dissertation, Virginia Polytechnic Institute and State University, Blacksburg, Virginia, 2004.